

Wearable flexible Kapton-graphene electromagnetic sensors

M. Bouherour^{a,*}, A. Nabila^a, L. Z. Meryem^{a,b}, T. Nourelhouda^a, R. Sawsen^a

^a*Laboratory of Electronic Materials Studies for Medical Applications (LEMEAMED), Faculty of Technology Sciences, Departement of Electronic, Frères MENTOURI Constantine University (FST-UMC), Algeria*

^b*Department of Physics Chemistry, Ecole normale supérieure "Assia DJEBAR" Constantine (ENSC), Algeria*

This research is dedicated to the development of a new technology for a quick diagnosis of viral virus, using electromagnetic technology facilitated by either a Rectangular Patch Resonator (RPR) or a Wearable Flexible Sensor (WFS) designed for non-invasive viral disease detection, including Nano-virus, and macro-virus. These devices is tailored for a precise and non-invasive detection of a wide array of viruses. To enhance diagnostic precision, an electromagnetic sensor was meticulously explored and simulated, to be capable of detecting and identifying even the most minuscule viruses. Employing numerical modeling with a focus on the 10 GHz to 20 GHz frequency range. We hold a strong sense of optimism regarding this sensor's potential for non-invasive virus detection. Extensive simulations conducted throughout this study have underscored the WFS's selectivity across all viruses, boasting an exceptional limit of detection and sensitivity. Moreover, the WFS exhibited the capability to distinguish between varying infection percentages, each corresponding to a distinct reflection pattern.

(Received February 13, 2024; Accepted April 25, 2024)

Keywords: Rectangular patch resonator (RPR), Wearable flexible sensor (WFS), Viral diseases, Dielectric parameters, Non-invasive control

1. Introduction

The evolution of real-time monitoring technologies has ushered in a new era of sensor development, integrating a multitude of analytical measures into versatile instruments applicable across diverse domains. These advancements have substantially enhanced the accuracy and efficiency with which various conditions can be identifying, thus enabling the early detection of issues that could lead to a higher rate of population recovery [1]. Notably, the rapid detection of a broad spectrum of nanomaterials, exhibiting superior sensitivities compared to their macroscopic counterparts and amenable fabrication processes, has presented a promising landscape for the development of such sensors, as illustrated in Figure 1, depicting the increasing trend in publications related to wearable electronics applications in recent years. These sensors encompass a wide array of chemical, physical, and optical attributes [2, 3].

Non-invasive devices have found widespread utility in the continuous real-time monitoring of various applications. Equipped with the ability to provide instantaneous data, these devices empower individuals to adapt their lifestyles, enhance their activities, improve their training regimens, and optimize their sleep patterns, among other use cases. Various sensors have been seamlessly integrated into wrist-wearable devices, finding application in diverse fields, including medicine, hazardous occupations, aviation, and emergency response systems [4]. The potential applications of wrist-wearable devices span:

Medicine: These devices play a pivotal role in monitoring a patient's health status, enabling the anticipation of potential health issues and the prevention of health deterioration. Of particular significance is the heightened interest in non-invasive sensors.

* Corresponding author: bouherour.mohamed@lec-umc.org
<https://doi.org/10.15251/JOBM.2024.162.89>

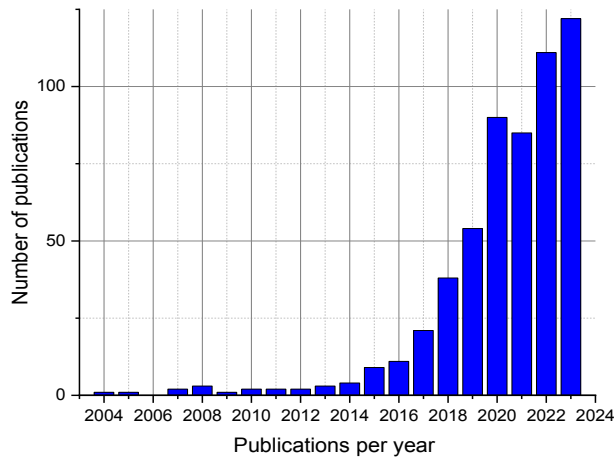


Fig. 1. Number of publications in PubMed per year with titles including non-invasive wearable electronics (Source: NCBI (National centre for Biotechnology information)).

In cases where suspicion arises, particularly within the framework of disease control and surveillance programs, samples are dispatched to specialized scientific research facilities, typically diagnostic laboratories. The field of virology has progressed significantly through the proliferation of molecular methods and techniques, coupled with enhanced clinical sensitivity in serological tests. The results obtained through these diagnostic endeavors play a pivotal role in the surveillance and management of both human and animal diseases.

Our approach focuses on the utilization of RPR, commonly associated with telecommunications, as sensors for medical Application. It is worth noting that RPR, traditionally characterized by rigidity and medium size, are engineering to fulfill their designated functions within the telecommunications domain [5]. However, in the realm of medical, a broader spectrum of requirements must be meeting. Consequently, our research endeavors to devise a sensor that combines flexibility, miniaturization, and the precision and sensitivity that equals or even surpasses the best sensors proposed in previous studies. The introduction of flexible and wearable sensors capable of being flexed, reconfigured, and twisted promises to significantly expand the scope of conventional electronic devices. The concept of miniaturization, while well-documented, remains an area of continual advancement and refinement [6].

Nevertheless, the endeavor to miniaturize wearable sensors, while preserving a low profile, ensuring design simplicity, facilitating seamless integration with circuits, and achieving the desired bandwidth, presents a formidable challenge that we are resolutely prepared to address.

2. Validation model design

Contemporary trends in the realm of non-invasive sensing methods have focused on investigating the sensitivity of the electromagnetic field, prompting our exploration of the RPR due to the prominence of its operational principles. The RPR comprises four fundamental components: a rectangular patch resonator, a substrate, a ground plane, and the feeding mechanism, as delineated in relevant literature [7].

The fundamental operation of the RPR hinges upon the excitation of the patch through a coaxial cable fixed on the ground plane, engendering an electric field that permeates the patch's surface continuously. This electric field extends beyond the boundaries of the patch, resulting in an external field known as the "Fringe field", this is chiefly governs the radiative properties of the patch. A phenomenon graphically elucidated in Figure 2.

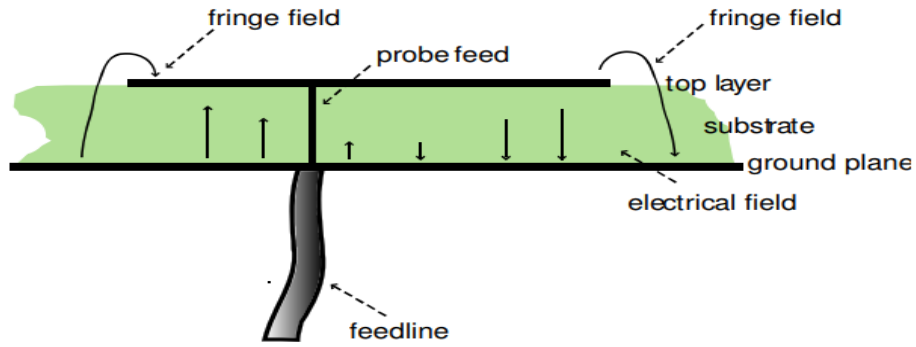


Fig. 2. Cross section of a patch antenna in its basic form [7].

For the optimal performance of the RPR, hereafter referred to as the Wearable Flexible Sensor (WFS) within this article, adherence to specific guidelines concerning its dimensions is imperative. Although we shall provide a concise overview of these dimension-related considerations in this article, an exhaustive examination of these parameters is beyond the scope of our present discourse.

The substrate's width of the RPR can be calculated by:

$$W = \frac{C}{2fr} \sqrt{\frac{2}{\epsilon_r + 1}}$$

Effective dielectric constant of the WFS is calculated as:

$$\epsilon_{eff} = \frac{\epsilon_r + 1}{2} + \frac{\epsilon_r - 1}{2} \left(\frac{1}{\sqrt{1 + \frac{2h}{W}}} \right)$$

The effective length is specified at the resonance frequency:

$$L_{eff} = \frac{C}{2fr\sqrt{\epsilon_{eff}}}$$

Extension length of the WFS compute with this equation:

$$\Delta L = h \times 0.412 \times \frac{(\epsilon_{eff} + 0.3) \left(\frac{W}{h} + 0.264 \right)}{(\epsilon_{eff} - 0.258) \left(\frac{W}{h} + 0.8 \right)}$$

The substrate's length "L" of the WFS is determinates as:

$$L = L_{eff} - 2\Delta L$$

The length of the RPR patch (L_p) can be calculated using the following formula:

$$L_p = \frac{\lambda}{1 - \frac{1}{\sqrt{\epsilon_r}}}$$

The width of the patch (W_p) can be determined using the following formula:

$$W_p = \frac{\lambda}{2 * \frac{\sqrt{\epsilon_r}}{Z_0 * \pi}}$$

The length of the RPR patch (L_p) can be calculated using the following formula:

$$F_r = \frac{c}{2 * L_p * \sqrt{\epsilon_r}}$$

where:

c: velocity of light, 3×10^8 m/s,

ϵ_r : dielectric constant of the substrate.

f_r : resonant frequency of antenna

h: Substrate thickness

Following rigorous computations and considerations, the critical dimensioning decisions have been deliberated upon and established. Specifically, we have decided to employ substrate dimensions measuring 10 mm in length and 9 mm in width, characterized by a thickness (h) of 0.32 mm. The patch, in turn, has been configured with dimensions of 4 mm by 3 mm. These selected dimensions assume a position of paramount significance in delineating the physical structure of the RPR. Their adoption is grounded in a comprehensive analysis that takes into account the resonant frequency and reflection coefficient, both of which play a pivotal role in the assessment of the RPR's operational efficiency.

To provide a more comprehensive understanding of the dimensions and their configuration, Figure 3 has been included, presenting these parameters from various vantage points. View (a) in the figure provides a frontal perspective, while view (b) accentuates the profile angle. The selection of these specific dimensions and specifications is the culmination of an exhaustive analytical process, meticulously undertaken to ascertain the RPR's capability to attain optimal performance concerning resonance and reflection characteristics. These dimension-related and parametric deliberations adhere to rigorous, methodical practices in accordance with established academic standards for the evaluation and design of the RPR.

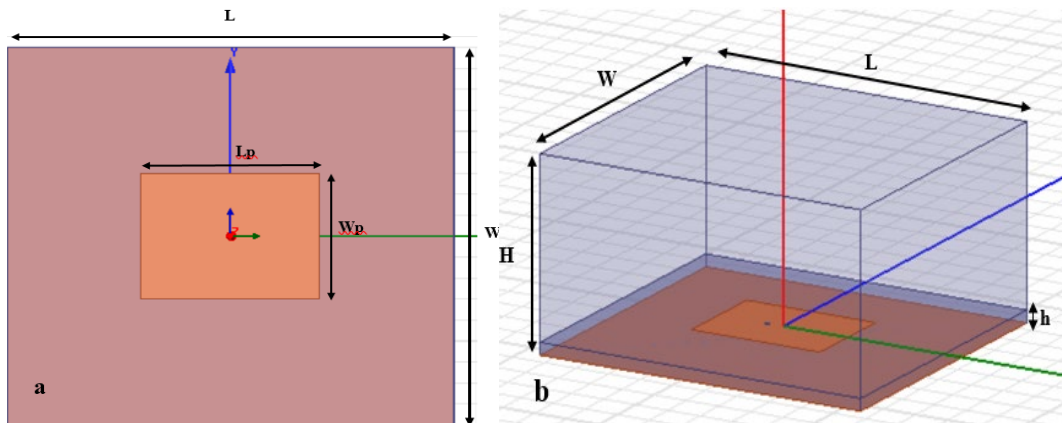


Fig. 3. RPR dimensions from different angles.

Table 1. Summary of the structure dimensions.

Dimensions	Size (mm)
L	10
W	9
Lp	4
Wp	3
h	0.32
H	5

3. Results and discussions

In order to use a rectangular patch resonator (RPR) as a wearable flexible sensor (WFS), it is necessary to choose one of its parameters and put it under detection conditions, and observe its variations. The RPR have several parameters that are related to the electromagnetic field and the radiation of its patch, the example Radiation Pattern, Antenna Gain, antenna efficiency, and reflection coefficient.

Our choice was to focus on the reflection coefficient also called return loss “S11” which is the parameter that represents the amount of power reflected by the RPR, which leads us to the power and sensitivity of the created electromagnetic field which is our goal from the beginning [9].

The Figure 04 below presents the reflection coefficient “S11” of the RPR presented above, where we took the most classical materials, a Perfect conductor for the patch and the Duroid for the substrate.

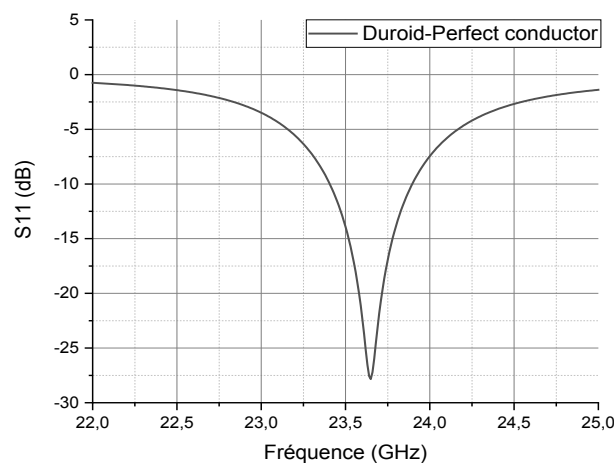


Fig. 4. RPR "S11" reflection coefficient Duroid-Perfect conductor.

The obtained results exhibit both conformity with the existing literature and a high level of satisfaction. In particular, the frequency response analysis unveils a prominent and distinct peak, characterized by a magnitude of -27.84 dB, showcasing minimal signal loss at a frequency of 23.6 GHz. Notably, this empirically determined resonant frequency closely approximates our theoretically anticipated value of 25 GHz, resulting in a fractional deviation ($\Delta f_r/f_r$) of 5.4%. This close correspondence serves as compelling evidence that affirms the resilience of our design approach and underscores the precision inherent in our computational calculations.

Numerous models have been developed to facilitate the selection of the new Wearable Flexible Sensor (WFS) and to fully harness its potential, with a focus on assessing their impact on the sensor's reflection coefficient, denoted as S11. This endeavor aims to achieve the desired outcomes that align with our research objectives. Our approach began with the exploration of alterations in the substrate material. In this context, we evaluated two rigid materials, specifically RT-Duroid 5880 and FR-4 epoxy, alongside two flexible materials, namely Polyimide film and benzocyclobutene (BCB). This assessment sought to attain the desired structural attributes for the WFS while maintaining the consistency of the patch and the grounding elements, with copper remaining as the common material component. The outcomes of these substrate material variations are visually depicted in Figure 5 below, providing a visual representation of the results obtained.

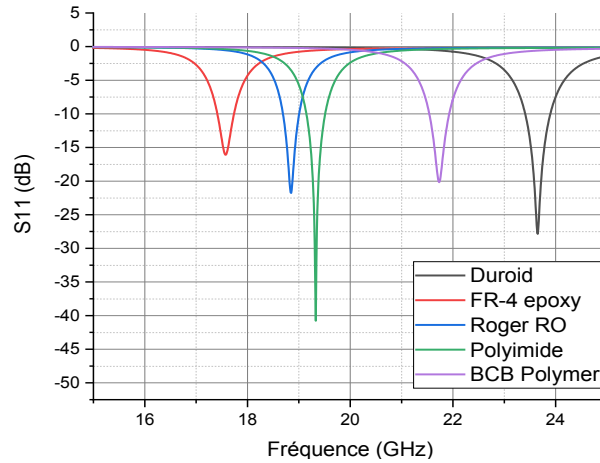


Fig. 5. Simulation results with different substrate materials.

To enhance the comprehensiveness of the results, we have opted to present them in a tabular format, as delineated in Table 02. This tabulation offers a convenient means for comparative analysis among the various materials. Within the table, we have collated key parameters for each material, including their permittivity (ϵ_r), reflection coefficient (S11), calculated resonant frequency, simulated resonant frequency, and the relative error ($\Delta f_r/f_r$). This structured presentation enables a more systematic and insightful assessment of the material characteristics and their influence on the sensor's performance.

Table 2. Detailed results of the RPR model simulation.

Materials	ϵ_r	S11 (dB)	Fr (GHz) Calculated	Fr (GHz) Simulated	$\Delta f_r/f_r$ (%)
Duroid	2.2	-27.84	25	23.65	5.4%
Rogers RO 4350	3.66	-21.76	19.6	18.85	3.8%
FR-4 epoxy	4.4	-16.07	17.9	17.57	1.8%
BCB Polymer	2.65	-20.17	23	21.73	5.52%
Polyimide	3.5	-40.77	20	19.33	3.3%

The evaluation of various substrate materials' performance is grounded in the assessment of two pivotal parameters: the reflection coefficient (S11), signifying the extent of power reflected by the sensor, and the relative error ($\Delta f_r/f_r$), which measures the accuracy of the resonant frequency.

A comparative analysis, based on the outcomes presented in Figure 05, unveils notable observations for the diverse materials considered:

1. Duroid Material: Frequently favored for standard Radiative Particle Radiation (RPR) designs due to its cost-effectiveness, Duroid demonstrates a reflection coefficient of -27.84 dB and a relative error of 5.4%, aligning reasonably well with the adopted transducer configuration.

2. Rogers RO 4550: This material showcases a reflection coefficient of -21.76 dB and a relative error of 3.8%, indicating commendable performance within the framework of this specific design.

3. FR-4 Epoxy: Commonly chosen for low-frequency applications, the FR-4 epoxy material yields a reflection coefficient of -16.07 dB and a relative error of 1.8% concerning the proposed design.

4. BCB Polymer: The BCB polymer material demonstrates a reflection coefficient of -20.17 dB and a relative error of 5.52%, thereby representing satisfactory performance within this context.

5. Polyimide (Kapton): Notably, the polyimide material, commonly referred to as Kapton, exhibits the most favorable reflection coefficient of -40.77 dB, establishing it as a highly suitable choice for standard RPR configurations. Furthermore, its relative error of 3.3% underscores its exceptional accuracy, solidifying its relevance in this domain.

In summary, the polyimide material stands out for its superior reflection coefficient and accuracy, while the other materials offer varying performance characteristics, making them viable options for specific RPR applications.

In our pursuit to investigate the influence of both patch and ground materials on sensor performance, we have made a deliberate choice to maintain the Polyimide film (Kapton) as the substrate material. This decision is founded on several key factors, including its flexibility, low relative error ($\Delta f/f$), and favorable reflection coefficient (S11), as illustrated in Figure 04. Subsequently, our focus has shifted towards varying the patch and ground materials. For this purpose, we have opted for materials characterized by high electrical conductivity, a factor that significantly impacts the reflection coefficient (S11). In this context, we have conducted assessments on four distinct materials, comprising two renowned perfect conductors, namely "Copper" and "Silver," which have been widely employed in prior research endeavors. Additionally, we have introduced one carbon-based materials, namely "Graphene" chosen for its exceptional electrical conductivity and high purity, as indicated in reference [9]. This selection has been made strategically to explore the intricate interplay between these material choices and their implications for the sensor's performance characteristics.

The assessment of the performance of the diverse patch and bulk materials is presented through the graphical representation in Figure 6. This figure illustrates the reflection coefficient plotted against the resonant frequency, providing a comprehensive visual depiction of the materials' characteristics.

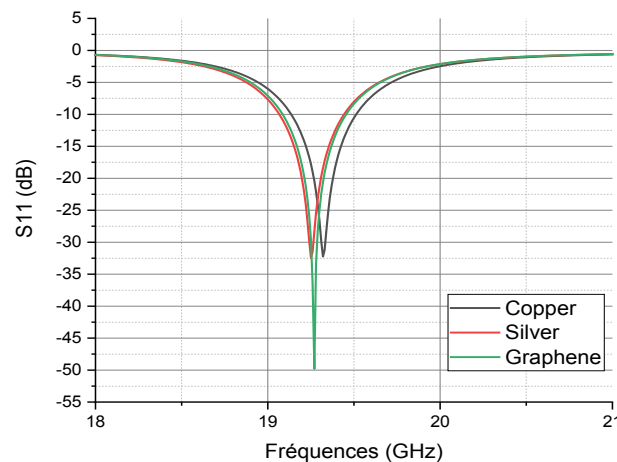


Fig. 6. RPR Simulation results with different patch materials.

Furthermore, a summary of these results is succinctly provided in Table 03. This table serves as a comprehensive reference, presenting key parameters for each material considered throughout the preceding phases of our study. These parameters encompass the values of electrical conductivity (σ), reflection coefficient (S11), and resonant frequency (Fr), offering a consolidated and easily accessible resource for a detailed comparison of the materials and their impact on sensor performance.

Table 3. Detailed results of the simulation.

Materials	σ (S/m)	S11 (dB)	Fr (GHz) Calculated	Fr (GHz) Simulated
Copper	58000000	-32.25	20	19.32
Silver	61000000	-32.46	20	19.25
Graphène	10^8	-49.82	20	19.27

Regarding the pivotal parameter of the reflection coefficient, a notable distinction emerged among the tested materials. Graphene exhibited a remarkably high reflection coefficient of -49.82 dB, surpassing the levels typically reported in the existing literature for these materials. This enhanced performance can be attributed to the intricacies of the geometry incorporated within the proposed model. In contrast, conventional materials like copper and silver demonstrated lower reflection coefficients, registering at -32.25 dB and -32.46 dB, respectively.

To benefit of their full potential and have the desired results that we seek for we decided to use the pair of Graphene and Kepton as materials for the patch and substrate respectively, for the final WFS model that it is used as a non-invasive applicator.

Conceived as a 2D material, graphene is essentially one of several layers stacked and bound by van der Waal forces to form graphite; its honeycomb-like shape gives it incredible strength while remaining very flexible, high stability, and superior electrical, optical, and mechanical properties, which we will detail in table 04 [10].

Whoever what is more interesting about this material is the fact that it is highly biocompatible, which leads us to say that is the impact of graphene on human health based on two parameters: biocompatibility and toxicity as well.

Recent studies have been able to evaluate the toxicity of graphene in target organs, including the immune system and the cardiovascular system, as well as in various kinds of organisms, such as bacteria. There is evidence that graphene layers can cross physiological barriers and reach secondary organs far from the initial entry [11].

Table 4. Graphene proprieties [12, 13.14.15].

Proprieties	Values
Intrinsic mobility(cm ² v-1 s-1)	200 000
Young's modulus (TPa)	~1.0
Electrical conductivity (S/m)	10^8
thermal conductivity (Wm-1K-1)	~5000
Hit support without structural damage (°C)	250
vapor-based synthesis (°C)	≈1000
Absorbance (%)	2.3
Optical transmittance (%)	~97.7

Kapton is a flexible insulating material that is stable even at high temperatures. It may be utilized in a wide range of applications that need superior electrical, mechanical, or thermal qualities, as shown in Table 05.

Kapton is commonly utilized in industrial applications that need exposure to high temperatures and high levels of vibration because of its ability to keep its unique mix of qualities under the most severe situations [16].

Table 5. Kapton proprieties [17].

Proprieties	Values
Tensile strength (MPa)	1231
Tensile modulus (GPa)	2.5
Density (kg/m ²)	1.42
Heat shrinkage (%)	0.17 (150°C)
Coef. of thermal expansion (ppm/°C)	20
Thermal conductivity (W/m·K)	0.12
Specific heat (J/g·K)	1.09
Degradation temperature (°C)	-269 and 400
Dielectric constant (-)	3.4

In the end, we come out with this final version of our WFS. A rectangular design with a Graphene patch and ground, and Kapton substrate. The figure 7 below will present the results that we had, we refined the frequency range from 18 GHz to 20.5GHz in order to have more accurate results, and his Q factor can be determined by the frequency spectrum, which is defined as

$$Q = f_r / \Delta f$$

where the resonance frequency f_r is the frequency at which the reflection coefficient S_{11} reaches its maximum, Δf is the width of the peak at its half height, so-called 3 dB bandwidth.[18]

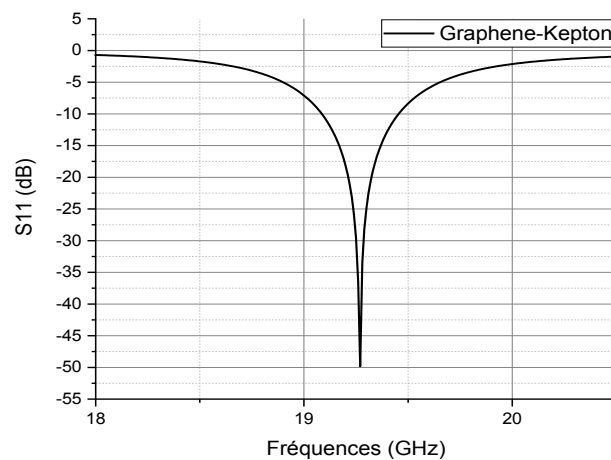


Fig. 7. Simulation results of the kapton-Graphene sensor.

The pair graphene-kepton, the first as patch and ground, and the second as substrate give an excellent result in terms of reflection coefficient as shown in figure 07, thanks to the compatibility of their magnificent properties that we listed in table 4 and 5.

As expected, the reflection coefficient decreased a little by giving -49.82 dB and a resonant frequency at 19.27 GHz, and a Q factor of 17.52 which is considered a very good result in relation to the standards of RPR results.

4. Conclusion

Our work was initiated with the primary objective of introducing a compact and flexible Wearable Preferment Sensor (WFS). The results presented throughout the various stages of this article substantiate the efficacy and quality of the WFS. Our WFS, tailored for non-invasive medical testing applications.

Significantly, the WFS demonstrates a robust response. The results obtained from the WFS are not only compelling but also meet our expectations, instilling a high level of confidence in its capabilities. These encouraging findings provide a compelling rationale for advancing into the implementation phase of the biosensor, reaffirming the potential of the WFS in the realm of medical diagnostics and nano-virus detection.

References

- [1] M. Bouherour, N. Aouabdia, M. Lamri Zeggar, N. H. Toudjen, S. Rouabah DJNB. Volume 17, 2022.173.705 ; <https://doi.org/10.15251/DJNB.2022.173.695>
- [2] N. Promphet, S. Ummartyotin, W. Ngeontae, P. Puthongkham, N. Rodthongkum, Anal. Chim. Acta, vol. 1179, no. 338643, p. 338643, 2021 ; <https://doi.org/10.1016/j.aca.2021.338643>
- [3] H. C. Ates et al., Nat. Rev. Mater., 2022 ; <https://doi.org/10.1038/s41578-022-00460-x>
- [4] S. Khan, S. Ali, A. Bermak, Sensors vol. 19, no. 5, p. 1230, 2019 ; <https://doi.org/10.3390/s19051230>
- [5] A. Y. I. Ashyap et al., IEEE Access, vol. 6, pp. 35214-35222, 2018 ; <https://doi.org/10.1109/ACCESS.2018.2847280>
- [6] H. Huang et al., Front. Chem., vol. 7, p. 399, 2019 ; <https://doi.org/10.3389/fchem.2019.00399>
- [7] Orban Microwave, Orban Microwave. [Online]. Available: <https://www.orbanmicrowave.com/>. [Accessed: 02-Aug-2022].
- [8] S.-E. Didi, I. Halkhams, M. Fattah, Y. Balboul, S. Mazer, M. E. Bekkali, Telkomnika, vol. 20, no. 3, p. 527, 2022 ; <https://doi.org/10.12928/telkomnika.v20i3.23159>
- [9] N. Ferdous, G. Chin Hock, S. Hamidah A.Hamid, M. N. A. Raman, T. Sieh Kiong, M. Ismail, IOP Conf. Ser. Earth Environ. Sci., vol. 268, no. 1, p. 012152, 2019 ; <https://doi.org/10.1088/1755-1315/268/1/012152>
- [10] C. Lee, X. Wei, J. W. Kysar, J. Hone, Science, vol. 321, no. 5887, pp. 385-388, 2008 ; <https://doi.org/10.1126/science.1157996>
- [11] H. Huang et al., Front. Chem., vol. 7, p. 399, 2019 ; <https://doi.org/10.3389/fchem.2019.00399>
- [12] C. Leow, P. B. Kreider, C. Notthoff, P. Kluth, A. Tricoli, P. Compston, Funct. Compos. Mater., vol. 2, no. 1, 2021 ; <https://doi.org/10.1186/s42252-020-00015-9>
- [13] C. Soldano, A. Mahmood, E. Dujardin, Carbon N. Y., vol. 48, no. 8, pp. 2127-2150, 2010 ; <https://doi.org/10.1016/j.carbon.2010.01.058>
- [14] Graphene and Graphene Oxide: Synthesis, Properties, and Applications
- [15] N. O. Weiss et al., Adv. Mater., vol. 24, no. 43, pp. 5782-5825, 2012 ; <https://doi.org/10.1002/adma.201201482>
- [16] J. Megusar, J. Nucl. Mater., vol. 245, no. 2-3, pp. 185-190, 1997 ; [https://doi.org/10.1016/S0022-3115\(97\)00012-3](https://doi.org/10.1016/S0022-3115(97)00012-3)
- [17] B. Y. Dharmadasa, M. McCallum, F. Lopez Jimenez, AIAA Scitech 2020 Forum, 2020 ; <https://doi.org/10.2514/6.2020-2165>
- [18] Handbook of Advanced Dielectric, Piezoelectric and Ferroelectric Materials, CRC Press, 2008.